

Mitigating Polarization Effects in On-Die Diffractive Optics for a CMOS Image Sensor

Christopher Thomas, Richard Hornsey

Dept. of Computer Science and Engineering, York University, Toronto, Canada

ABSTRACT

On-die optics have been proposed for stand-alone image sensors. Previous works by the authors have proposed fabricating diffractive optical elements using the upper metal layers in a commercial CMOS process. This avoids the cost associated with process steps associated with microlens fabrication, but results in a point spread function that varies with the wavelength, angle, and polarization of incident light. Wavelength and angle sensitivities have been addressed by previous works. This paper models the effects of polarization on the point spread function of the imaging system, and proposes optical and algorithmic methods for compensating for these effects. The imaging behaviors of the resulting systems are evaluated. Simulations indicate that the uncorrected system can locate point sources to within ± 0.1 radian, and polarized point sources to within ± 0.05 radian along the axis of polarization. A system is described that uses a polarization-insensitive optical element and a deconvolution filter to achieve a corrected resolution pf ± 0.05 radian, with the ability to perform imaging of non-point sources with white light illumination.

Keywords: CMOS image sensors, microlenses, diffractive optics, image processing, polarizers

1. INTRODUCTION

The technique of integrating on-die optics into image sensors has been widely used for improving fill factor in CMOS active pixel sensors.^{1,2} In recent years, on-die optics have also been used to construct standalone sensors for a variety of applications, including imaging.³⁻⁵ However, fabrication of on-die optics typically requires additional process steps, which increase the cost of fabrication.

To address the problem of cost, the authors in previous works describe a method of using the metal layers in a standard CMOS process to fabricate diffractive optics.^{6,7} A diagram of this type of sensor is shown in Figure 1. Aberrations introduced, and an approach to correcting them using deconvolution, were discussed. This paper extends these past results to take into account the fact that the optical elements fabricated are made of a conducting material, which has polarizing effects. The effects of polarization on point spread functions of the optics are discussed, and methods for mitigating these effects are presented.

Section 2 describes the optical system being studied, modelling both the physical system and the deconvolution processing step. Section 3 describes the effect of polarization on Fresnel zone plate point spread functions. Section 4 describes alternative optical elements that are less affected by polarization, and characterizes their behavior. Section 5 applies deconvolution to partially compensate for artifacts introduced by the optical elements. Results are summarized in Section 6.

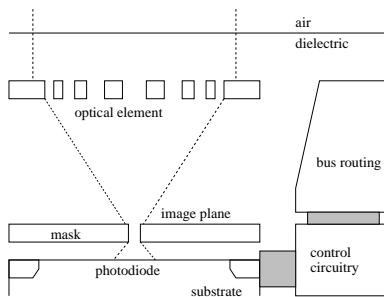


Figure 1. CMOS pixel with diffractive optics.

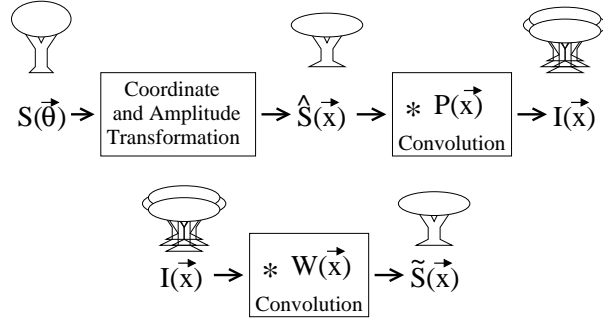


Figure 2. System block diagram.

2. SYSTEM MODEL

The imaging system is modelled as shown in Figure 2. The optics are modelled as performing a coordinate transformation and intensity scaling on the scene contents S , followed by convolution with a point spread function P , resulting in the image I . The post-processing step produces a reconstructed scene \tilde{S} by convolving the image I with a reconstruction filter W . The goal is for the reconstructed scene \tilde{S} to match the transformed scene \hat{S} , or a desired subset thereof, as closely as possible. Equations 1 through 3 describe this transformation.

$$\hat{S}(\vec{x}) = T_{amp}(\vec{x})S(T_{ang}(\vec{x})) \quad (1)$$

$$I(\vec{x}) = \hat{S}(\vec{x}) * P(\vec{x}) \quad (2)$$

$$\tilde{S}(\vec{x}) = I(\vec{x}) * W(\vec{x}) \approx \hat{S}(\vec{x}) \quad (3)$$

Numerical calculation of the point spread function P is discussed in Section 2.1, and the deconvolution approach used to derive W is discussed in Section 2.2. These are extensions of techniques used in previous works by the authors.⁷

2.1. Optical System

Point spread functions were computed in previous works as a function of the wavelength and angle of incidence of light falling on the sensor's optics.⁷ The algorithm used is illustrated in Figure 3. For each angle and wavelength of incident light, a plane wave of appropriate intensity is considered. The amplitude and phase of the incident light is computed at each point on the optical element, taking into account refraction by the inter-layer dielectric. The optical element is then used to mask the plane wave. For the algorithm used in previous years, the metal grating is assumed to either perfectly transmit or perfectly block the plane wave, with no phase shift introduced. Each point in the masked plane wave is considered to be a point source of light, emitting with intensity scaled to $1/r^2$ and a phase shift proportional to r . The intensity and phase shift pattern formed on the image plane by one point source is convolved with the masked plane wave's intensity and phase pattern to find the point spread function of the original incident plane wave. This method was a crude approximation of interference of isotropic radiators. A more accurate variant considers isotropic radiators emitting with intensity scaled by $1/r$ and phase shift scaled by r .⁸ The intensity and phase shift pattern formed on the image plane by the isotropic radiator is then convolved with the masked plane wave's intensity and phase. The squared magnitude of the resulting complex point spread function is taken to produce the measured point spread function (corresponding to the expectation value associated with the complex wavefunction).

The algorithm used in this work is shown in Figure 4. Point spread functions are sensitive to the angle, wavelength, and polarization of incident light. For each angle and wavelength of incident light, a plane wave of appropriate intensity is considered. The amplitude, phase, and polarization of the incident plane wave are computed at each point on the optical element, taking into account refraction by the inter-layer dielectric. Rather

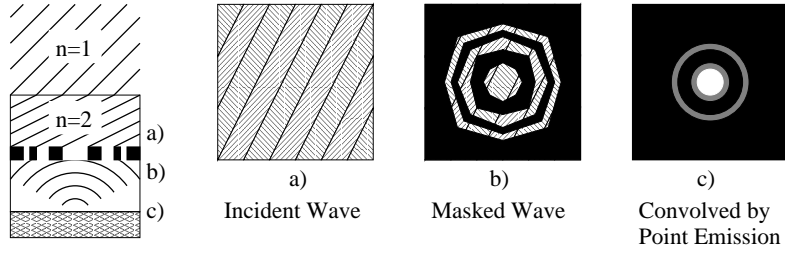


Figure 3. Isotropic emission image-forming algorithm (2007).

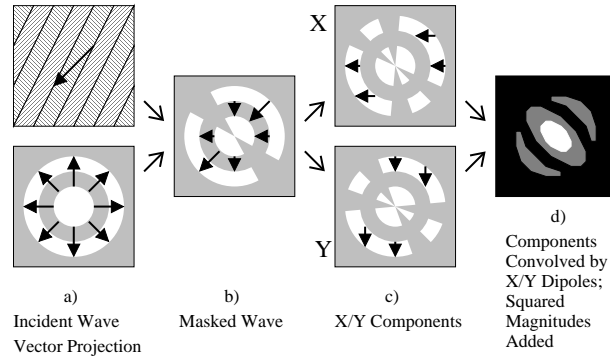


Figure 4. Dipole emission image-forming algorithm (2008).

than being a scalar, the intensity and phase of the wave are expressed as a vector at each point, representing the intensity and phase of polarization components aligned with the X and Y axes of the optical element. The Z component is assumed to be reflected by the optical element and is ignored.

The optical element also has a vector field associated with it, representing the polarization direction that the optical element passes at each point on its surface. The vector projection of the incident plane wave's polarization vector onto the optical element's polarization vector gives a vector field representing the transmitted amplitude and phase at every point on the optical element after polarization by the element, with components aligned with the X and Y axes. This modified vector field is masked by the optical element's transparency mask to produce the transmitted vector field. Filled areas of the optical element are assumed to perfectly reflect all polarization components, while gaps in the grating are assumed to act as perfect polarizing filters with no phase shift.

Each point in the X and Y masked plane wave components is treated as a dipole emitter, emitting with a far field intensity proportional to $\sin(\theta)/r$,⁸ and a phase shift proportional to r . The intensity and phase shift patterns formed on the image plane by X and Y-aligned dipoles are convolved with the corresponding masked plane waves' intensity and phase patterns to find the point spread functions of the X and Y components of the original incident plane wave. The squared magnitudes of these complex point spread functions are then taken, and added to each other, to produce the measured point spread function (corresponding to the expectation value associated with the complex wavefunctions).

2.2. Post-Processing

As described by Equations 1 and 2 in Section 2, the image-forming process is treated as a transformation of spatial coordinates and intensity, followed by a convolution by a point spread function. Reversing the space-domain transformation described by Equation 1 is straightforward, given that T_{amp} and T_{ang} can be easily derived via simulation or via calibration measurements from actual devices. Previous simulations indicated that the

angle transformation was approximately linear over the domain of interest,⁷ meaning it could even be ignored, with usable images still being produced. The most important artifact to be corrected is therefore the blurring described by Equation 2.

Deblurring the image and separating out channels of interest (such as specific colors or polarization axes) is performed using a variant of Wiener deconvolution. Wiener deconvolution was chosen in previous works for this purpose because it gives the smallest mean squared error between original and reconstructed scenes when the point spread function and noise functions are both known.⁹ Application of Wiener filtering to images produced using the isotropic radiation simulation described in Section 2.1 succeeded in resolving image details that had been blurred.⁷ The approach used is described here, and extensions aimed at suppressing noise and separating channels are added.

The point spread function is modelled as the combination of an ideal point spread function $P(\vec{x})$ and a noise function $N_p(\vec{x})$ that represents changes in the point spread function across wavelength, angle of incidence, and polarization. This alters Equations 2 and 3 to produce Equations 4 and 5, respectively:

$$I(\vec{x}) = \hat{S}(\vec{x}) * (P(\vec{x}) + N_p(\vec{x})) \quad (4)$$

$$\tilde{S}(\vec{x}) = \hat{S}(\vec{x}) * P(\vec{x}) * W(\vec{x}) + \hat{S}(\vec{x}) * N_p(\vec{x}) * W(\vec{x}) \quad (5)$$

Moving to the frequency domain, the squared error is expressed as:

$$\epsilon^2(\vec{\omega}) = \left(\hat{S}(\vec{\omega})P(\vec{\omega})W(\vec{\omega}) + \hat{S}(\vec{\omega})N_p(\vec{\omega})W(\vec{\omega}) - \hat{S}(\vec{\omega}) \right)^2 \quad (6)$$

$$\epsilon^2(\vec{\omega}) = \left(\hat{S}(\vec{\omega}) \right)^2 [(P(\vec{\omega}) + N_p(\vec{\omega}))W(\vec{\omega}) - 1]^2 \quad (7)$$

The mean squared error is the integral of $\epsilon^2(\vec{\omega})$ across $\vec{\omega}$. Minimizing the mean squared error without a priori knowledge of the transformed scene $\hat{S}(\vec{\omega})$ requires setting the derivative with respect to $W(\vec{\omega})$ of $\epsilon^2(\vec{\omega})$ to zero for all $\vec{\omega}$:

$$0 = \frac{d}{dW(\vec{\omega})}[\epsilon^2(\vec{\omega})] = 2(\hat{S}(\vec{\omega}))^2 [(P(\vec{\omega}) + N_p(\vec{\omega}))W(\vec{\omega}) - 1] (P(\vec{\omega}) + N_p(\vec{\omega})) \quad (8)$$

The only term that can be manipulated is the one containing $W(\vec{\omega})$. Setting this to zero produces the Wiener deconvolution filter for this description of the system:

$$0 = (P(\vec{\omega}) + N_p(\vec{\omega}))W(\vec{\omega}) - 1 \quad (9)$$

$$W(\vec{\omega}) = \frac{1}{P(\vec{\omega}) + N_p(\vec{\omega})} \quad (10)$$

Previous work found that this did not adequately suppress noise.⁷ Artifacts appeared that were interpreted as being amplified components of inadequately characterized point spread function variation noise. This form of noise is addressed by two methods. First, a tuning parameter is added to explicitly increase suppression of the known noise function $N_p(\vec{\omega})$. Second, a clipping function is applied to prevent the normalized magnitude of $W(\vec{\omega})$ from exceeding a chosen amplification threshold. This acts to suppress noise components introduced that were not incorporated into $N_p(\vec{\omega})$. The resulting modified filter is described by Equation 11:

$$W(\vec{\omega}) = \text{Clip} \left(\frac{1}{P(\vec{\omega}) + K_n N_p(\vec{\omega})} \right) \quad (11)$$

The space-domain point spread function $P(\vec{x})$ and the PSF noise function $N_p(\vec{x})$ are evaluated numerically. $P(\vec{x})$ is either specified to be the simulated point spread function for some representative angle, wavelength, and polarization, or is specified to be the numerically integrated value of the simulated point spread function over some domain of interest. For point spread functions that vary angle of incidence (and hence displacement in \vec{x}), this integration is performed after centering the point spread function such that its centroid is always at the origin. After the point spread function $P(\vec{x})$ is chosen, the noise function $N_p(\vec{x})$ is computed via a similar numerical integration across the domain of valid values of angle, wavelength, and polarization. The quantity being integrated is the squared difference between the point spread function for each specific angle, wavelength,

and polarization, and the representative point spread function $P(\vec{x})$. After integration, the root mean squared difference is computed as a function of \vec{x} , and used as $N_p(\vec{x})$.

Separation of red, green, and blue channels in the image was previously attempted by use of Fresnel zone plates tuned to red, green, and blue wavelengths.⁷ This approach is not viable for separation of polarization components, which are not selectively suppressed or enhanced by the optics considered in Sections 3 or 4. Separation with a single type of optical element is considered by revisiting the Wiener filter derivation. The scene, image, and point spread function are considered to be functions of not only \vec{x} , but of components of parameter space, collectively specified by \vec{y} . For purposes of this paper, \vec{y} specifies the wavelength and polarization of the incident light. Equations 4 and 5 become Equations 12 and 13, respectively:

$$I(\vec{x}) = \int_Y \hat{S}(\vec{x}, \vec{y}) * (P(\vec{x}, \vec{y}) + N_p(\vec{x}, \vec{y})) dy \quad (12)$$

$$\tilde{S}(\vec{x}, \vec{y}) = W(\vec{x}, \vec{y}) * \int_Y \hat{S}(\vec{x}, \vec{y}) * (P(\vec{x}, \vec{y}) + N_p(\vec{x}, \vec{y})) dy \quad (13)$$

Consider parameter space divided into domains Y_1, Y_2, \dots, Y_n . For each Y_k , consider there to be a fixed point spread function $P_k(\vec{x})$ and noise function $N_{p_k}(\vec{x})$. Equation 12 becomes:

$$I(\vec{x}) = \sum_{k=1}^n \left[(P_k(\vec{x}) + N_{p_k}(\vec{x})) * \int_{Y_k} \hat{S}(\vec{x}, \vec{y}) dy \right] \quad (14)$$

For the sake of convenience, the integral of $\hat{S}(\vec{x}, \vec{y})$ over Y_k is designated $\hat{S}_k(\vec{x})$. Equation 14 becomes:

$$I(\vec{x}) = \sum_{k=1}^n \hat{S}_k(\vec{x}) * (P_k(\vec{x}) + N_{p_k}(\vec{x})) \quad (15)$$

And Equation 13 becomes:

$$\tilde{S}_m(\vec{x}) = W_m(\vec{x}) * \sum_{k=1}^n \hat{S}_k(\vec{x}) * (P_k(\vec{x}) + N_{p_k}(\vec{x})) \quad (16)$$

In the frequency domain, the squared error for channel m is:

$$\epsilon_m^2(\vec{\omega}) = \left(W_m(\vec{\omega}) \sum_{k=1}^n \hat{S}_k(\vec{\omega}) (P_k(\vec{\omega}) + N_{p_k}(\vec{\omega})) - \hat{S}_m(\vec{\omega}) \right)^2 \quad (17)$$

Taking the derivative with respect to $W_m(\vec{\omega})$ and setting this to zero gives the channel's Wiener filter:

$$0 = \frac{d}{dW_m(\vec{\omega})} [\epsilon_m^2(\vec{\omega})] = 2 \left[W_m(\vec{\omega}) \sum_{k=1}^n \hat{S}_k(\vec{\omega}) (P_k(\vec{\omega}) + N_{p_k}(\vec{\omega})) - \hat{S}_m(\vec{\omega}) \right] \left[\sum_{k=1}^n \hat{S}_k(\vec{\omega}) (P_k(\vec{\omega}) + N_{p_k}(\vec{\omega})) \right] \quad (18)$$

$$0 = W_m(\vec{\omega}) \sum_{k=1}^n \hat{S}_k(\vec{\omega}) (P_k(\vec{\omega}) + N_{p_k}(\vec{\omega})) - \hat{S}_m(\vec{\omega}) \quad (19)$$

$$W_m(\vec{\omega}) = \frac{1}{\sum_{k=1}^n \left(\frac{\hat{S}_k(\vec{\omega})}{\hat{S}_m(\vec{\omega})} \right) (P_k(\vec{\omega}) + N_{p_k}(\vec{\omega}))} \quad (20)$$

Separating out the summation term where $k = m$ allows a noise suppression coefficient K_n to be added:

$$W_m(\vec{\omega}) = \text{Clip} \left(\frac{1}{P_m(\vec{\omega}) + K_n N_{p_m}(\vec{\omega}) + K_n \sum_{k \neq m} \left(\frac{\hat{S}_k(\vec{\omega})}{\hat{S}_m(\vec{\omega})} \right) (P_k(\vec{\omega}) + N_{p_k}(\vec{\omega}))} \right) \quad (21)$$

Numerical evaluation of this filter requires one additional assumption. The values of $\hat{S}_k(\vec{\omega})$ and $\hat{S}_m(\vec{\omega})$ aren't known a priori. These provide a weighting coefficient for various parts of the domain Y :

$$\frac{\hat{S}_k(\vec{\omega})}{\hat{S}_m(\vec{\omega})} = \frac{\int_{Y_k} \hat{S}(\vec{w}, \vec{y}) dy}{\int_{Y_m} \hat{S}(\vec{w}, \vec{y}) dy} \quad (22)$$

For purposes of this paper, this ratio is assumed to be equivalent to:

$$\frac{\hat{S}_k(\vec{\omega})}{\hat{S}_m(\vec{\omega})} \approx \frac{\int_{Y_k} 1 dy}{\int_{Y_m} 1 dy} \quad (23)$$

A more elaborate approach is to perform successive approximation of the weighting coefficients based on deconvolved estimates of $\hat{S}(\vec{w}, \vec{y})$. This is left as an avenue for future work.

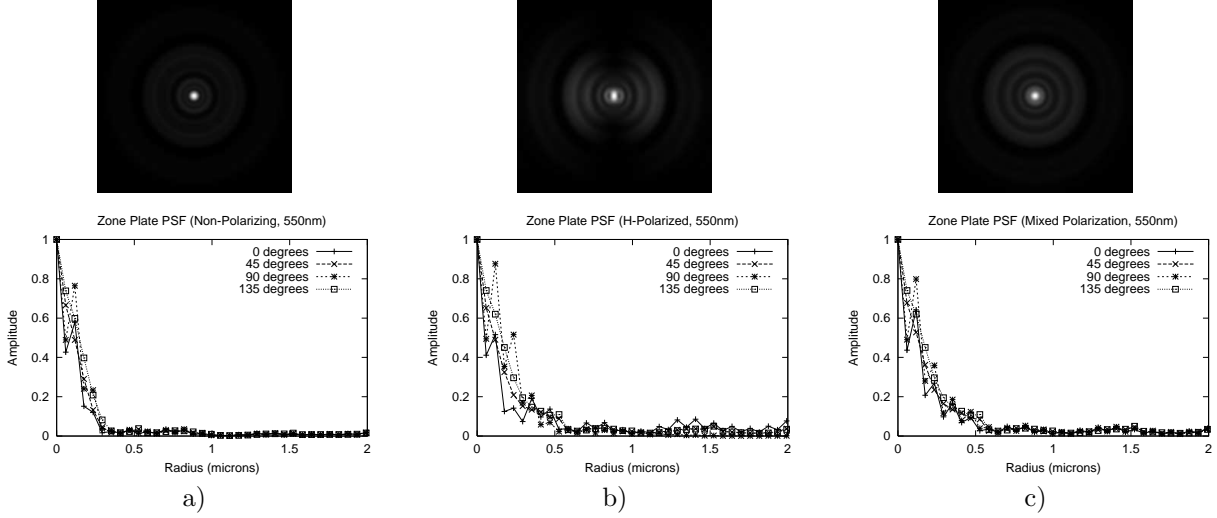


Figure 5. Zone plate point spread functions for a) non-polarizing plate, b) horizontally-polarized light, and c) mixture of polarizations.

3. FRESNEL ZONE PLATE OPTICS

Previously, Fresnel zone plate optics were treated as not affecting the polarization of incident light.⁷ This results in the point spread function shown in Figure 5a), and the modulation transfer function shown in Figure 6a). Applying horizontally-polarized light and dipole-based radiation patterns produces the point spread function in Figure 5b) and modulation transfer function in Figure 6b). As expected, focusing is strong only in the direction of polarization. Modelling incident light as containing a uniform mixture of polarizations produces the point spread function and modulation transfer function shown in Figures 5c) and 6c), respectively.

From point spread function profile plots, the full-width half-maximum (FWHM) spot size for the non-polarizing and mixed-polarization point spread functions is approximately 0.4 microns on the image plane, dominated by the first fringe surrounding the central point. The central peak has diameter of approximately 0.2 microns on the image plane. This is consistent with modulation transfer function values, which show a dropoff at approximately wavenumber 70 (corresponding to a sampling interval of about 0.14 microns on the 20-micron field simulated). The FWHM spot size for the horizontally-polarized point spread function varies from 0.2 to 0.4 microns, depending on the angle at which it is measured. This is consistent with the modulation transfer function value for this point spread function, which shows a dropoff at about wavenumber 40 on the Y axis and about 70 on the X axis. These wavenumbers correspond to sampling intervals of about 0.14 and 0.25 microns, respectively. Angular resolution for a FWHM spot size of 0.4 microns is about 0.16 radian (refractive index of 2, focal length of 5 microns, for the region between the optical element and the sensor's image plane).

Point spread function and modulation transfer function responses to illumination wavelength are shown in Figures 7a) and 8a), respectively. As expected with a diffractive optical element, the PSF and MTF are strongly wavelength-dependent. For a zone plate tuned to green wavelengths (550 nm), spot FWHM with mixed polarization is about 0.4 microns for green and blue light, and about 1.0 micron for red light (due to fringes). Spectral features are broadly similar for red, green, and blue wavelengths, with a dropoff at wavenumber 60 (red), 70 (green), or 80 (blue). However, response at any given frequency can vary by an order of magnitude or more, due to the presence of multiple notches in the low-frequency response that vary with wavelength.

Point spread function and modulation transfer function responses to angular displacement of the point source being imaged are shown in Figures 7b) and 8b), respectively. Spectral features, including notches, are very similar for centered and displaced sources. The central part of the point spread function also remains the same, with a FWHM of about 0.4 microns in both cases. Fringe amplitude is much higher in the displaced case, however, degrading spot diameter to about 0.8 microns at 0.3 of the maximum (vs. 0.6 microns for the centered case).

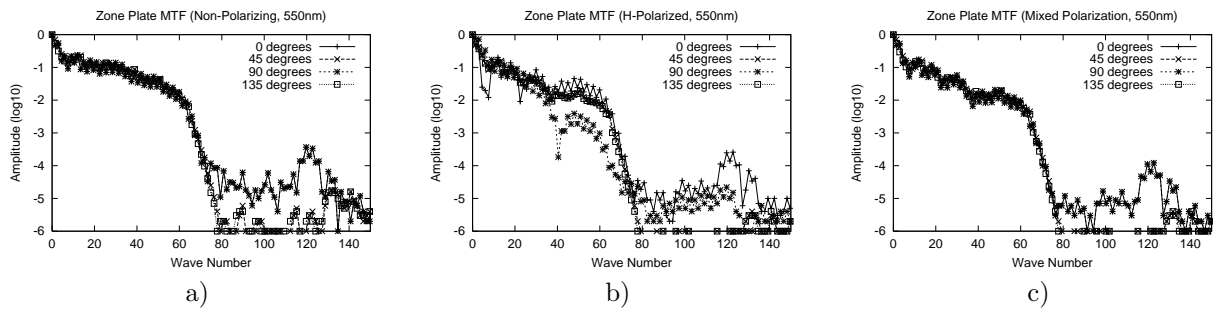


Figure 6. Zone plate modulation transfer functions for a) non-polarizing plate, b) horizontally-polarized light, and c) mixture of polarizations.

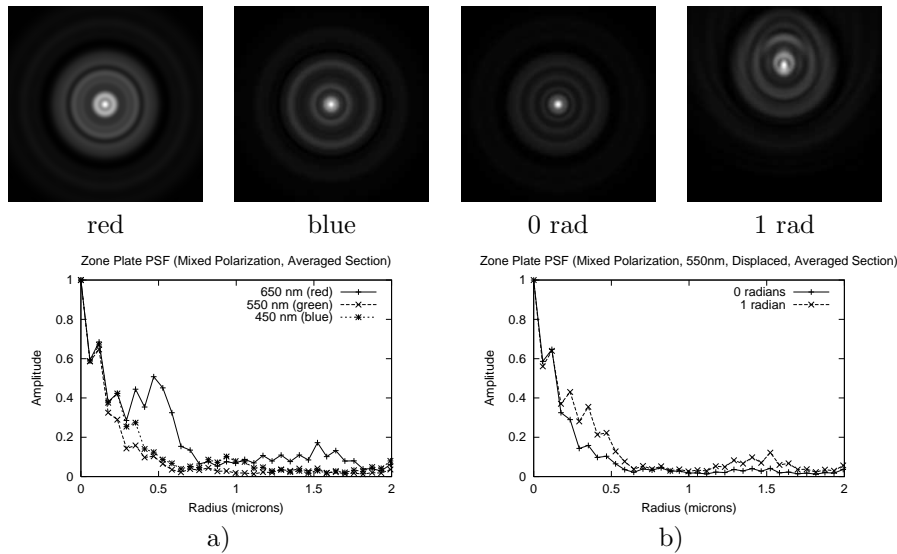


Figure 7. Zone plate point spread functions vs a) wavelength and b) displacement.

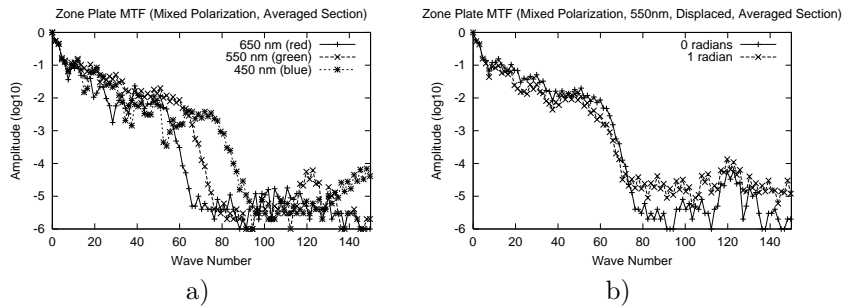


Figure 8. Zone plate modulation transfer functions vs a) wavelength and b) displacement.

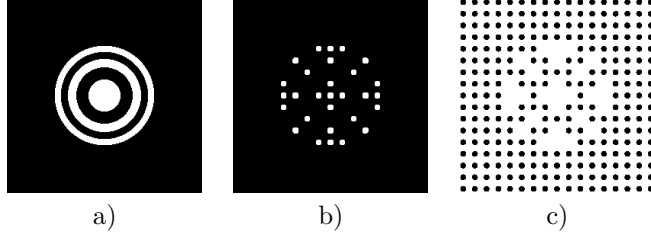


Figure 9. a) Zone plate, b) hole plate, and c) dot plate optical elements.

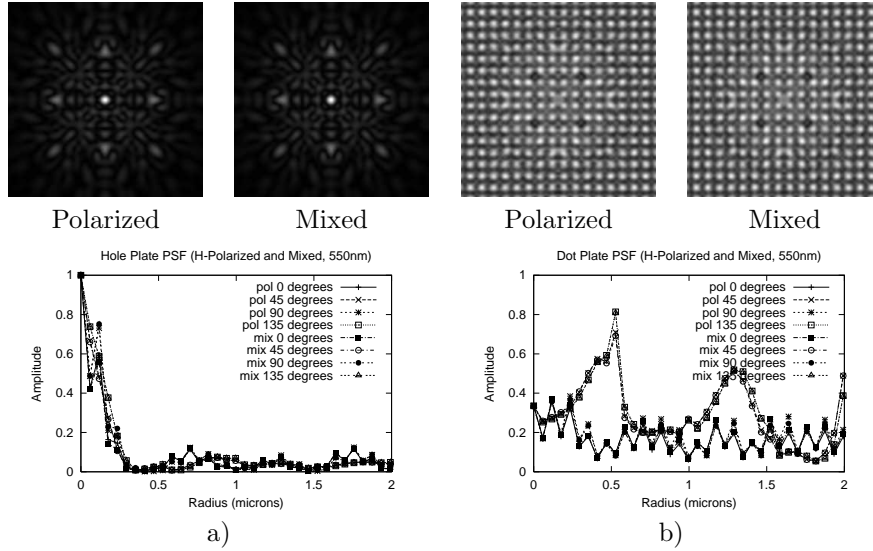


Figure 10. Point spread functions for a) hole plate and b) dot plate, for horizontally-polarized light and a mixture of polarizations.

4. HOLE AND DOT OPTICS

The difficulty with Fresnel zone plate optics is that the point spread function and modulation transfer function are sensitive to the polarization, as shown in Figures 5 and 6, respectively. Deconvolution via Wiener filtering requires that the PSF (or MTF) be known in advance, without knowledge of details of the scene being imaged (such as the illumination polarization). To mitigate the problem of polarization sensitivity, two new optical elements are studied: an array of holes, and an array of dots, each configured to act like a Fresnel zone plate. These optical elements are shown in Figure 9. Neither of these optical elements is expected to act as a polarizing filter, due to the absence of structures that conduct preferentially along one axis. The hole plate is expected to reflect most light, but to allow a small amount of the light striking the holes to pass, while the dot plate is expected to pass most light.

Modelled point spread functions for hole and dot plates are shown in Figure 10a) and 10b), respectively. Both succeed in being insensitive to polarization. However, the dot plate has enough aliasing to seriously hamper deconvolution efforts. Further discussion focuses on the hole plate.

From the point spread function profile plots, the full-width half-maximum spot size for the hole plate is approximately 0.4 microns on the image plane. The modulation transfer function shows a dropoff at approximately wavenumber 60, corresponding to a sampling interval of 0.17 microns on the 20-micron field simulated. Angular resolution for a FWHM spot size of 0.4 microns is about 0.16 radian (with refractive index 2 and focal length 5 microns). However, the secondary peaks in the point spread function result in substantial aliasing in uncorrected images formed by this optical element. Deconvolution of these artifacts is discussed in Section 5.

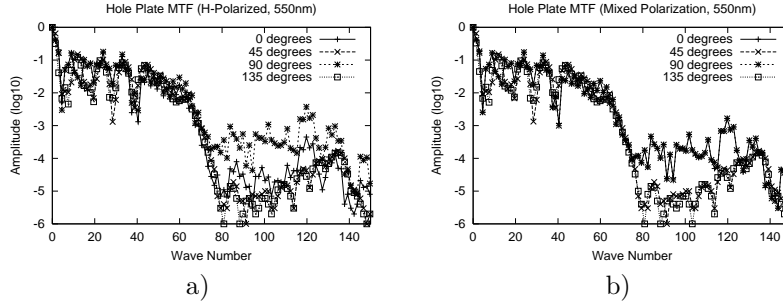


Figure 11. Hole plate modulation transfer functions for a) horizontally-polarized light and b) mixture of polarizations.

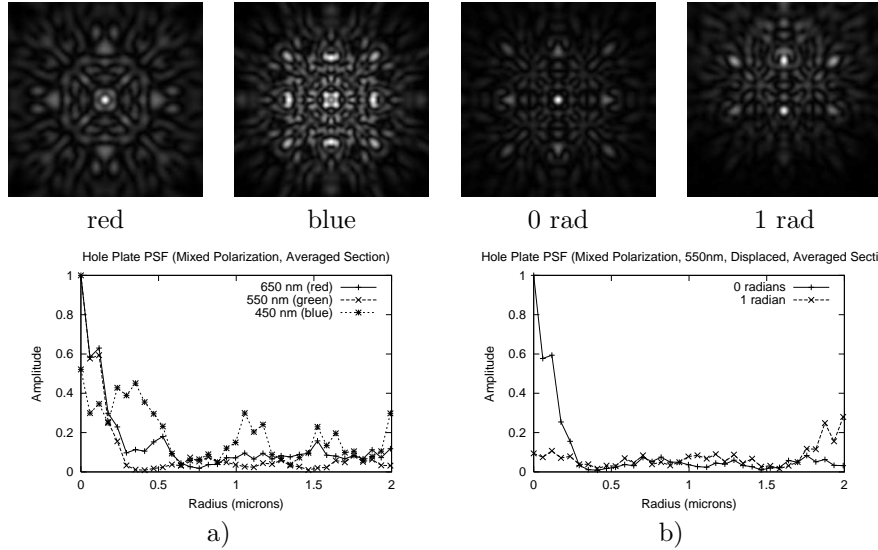


Figure 12. Hole plate point spread functions vs a) wavelength and b) displacement.

Hole plate point spread function and modulation transfer function responses to illumination wavelength are shown in Figures 12a) and 13a), respectively. The PSF and MTF are very wavelength-dependent, as expected for an optical element containing a periodic pattern. For a hole plate designed for green wavelengths (550 nm), spot FWHM with mixed polarization is about 0.4 microns for red and green light, and about 1.0 micron for blue light. Strong secondary peaks also occur with blue light. Spectral features are broadly similar across illumination wavelengths, with MTF dropoffs at wavenumbers of about 50 (red), 60 (green), or 80 (blue). As with the zone plate discussed in Section 3, MTF response at any given wavenumber can vary across at least an order of magnitude as illumination wavelength is changed, due to notch patterns in the low-frequency response.

Point spread function and modular transfer function responses to angular displacement of the point source being imaged are shown in Figure 12b) and 13b), respectively. Spectral features, including notches, are very similar for centered and displaced sources. The central part of the point spread function also remains the same, with a FWHM of about 0.4 microns in both cases. However, secondary peaks in the point spread function are stronger in the displaced case, causing aliasing problems in images with wide fields of view.

5. DECONVOLUTION

Following the methods described in Section 2.2, a deconvolution filter was obtained. The effects of this deconvolution filter on the point spread functions of zone plate and hole plate optics are shown in Figure 14. A more quantitative depiction is in the modulation transfer function and point spread function plots in Figures 15

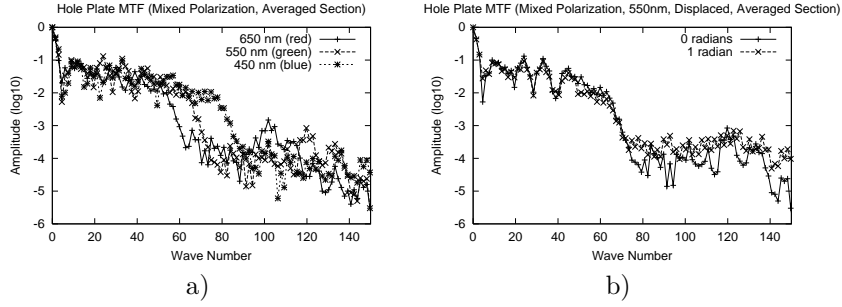


Figure 13. Hole plate modulation transfer functions vs a) wavelength and b) displacement.

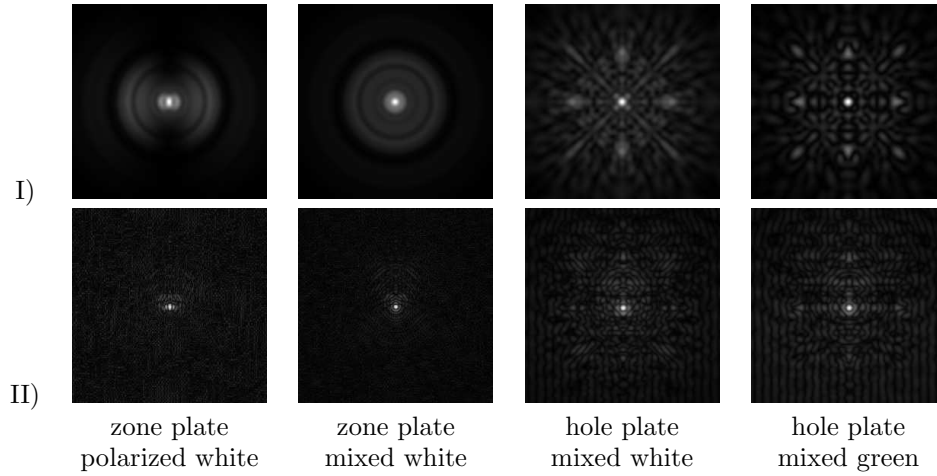


Figure 14. Point spread functions I) before and II) after deconvolution.

and 16. The full-width half-maximum of the point spread function is reduced to approximately 0.2 micron via suppression of secondary fringes, corresponding to an angular resolution of less than 0.1 radian (with a refractive index of 2 and a focal length of 5 microns). The modulation transfer function is transformed into a plateau, equalizing spectral components out to approximately 70 to 80 wavenumbers, which is consistent with this spot size (sampling interval of about 0.12 micron, with a field size of 20 microns). Higher spatial frequencies are likely to be spurious, as the small size of the optical element limits resolution to approximately 0.1 radian (the aperture diameter is 10 microns or less).

The modulation transfer function of the deconvolved hole plate doesn't drop off after 80 wavenumbers, but instead rises. This has the effect of amplifying noise and other unwanted artifacts, which is visible in Figure 14. This is compensated for by manually introducing a low-pass filter into the deconvolution function, which reduces the noise to the levels seen in Figures 14. These unwanted high-frequency components are the primary source of noise in reconstructed images. Sample images are found in Figure 17; the deconvolved images are legible for both zone plate and hole plate optics.

6. CONCLUSIONS

In conclusion, this work presents a more accurate approach to modelling the imaging behavior of the on-die diffractive optics system previously proposed by the authors.⁶ The Fresnel zone plate optics originally proposed are strongly affected by polarization, with spot size and resolution varying by a factor of two for focusing parallel to or perpendicular to the axis of polarization. Uncorrected image resolution parallel to the polarization axis is

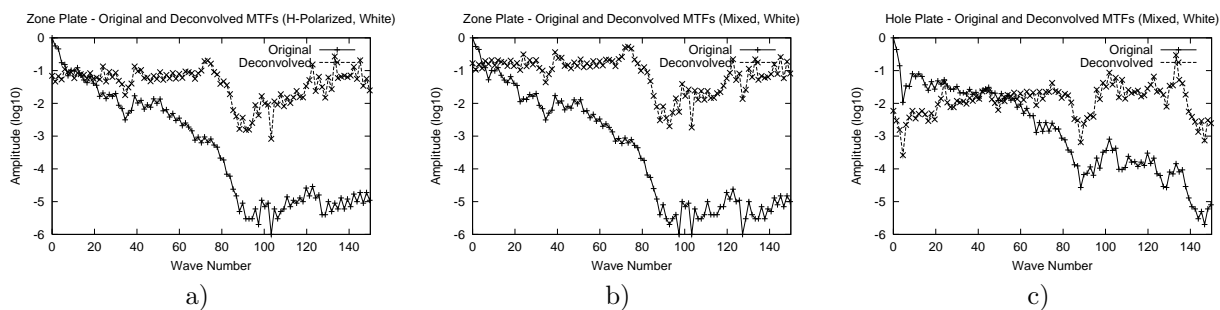


Figure 15. Original and deconvolved modulation transfer functions for a) a zone plate with polarized white light, b) a zone plate with mixed white light, and c) a hole plate with mixed white light.

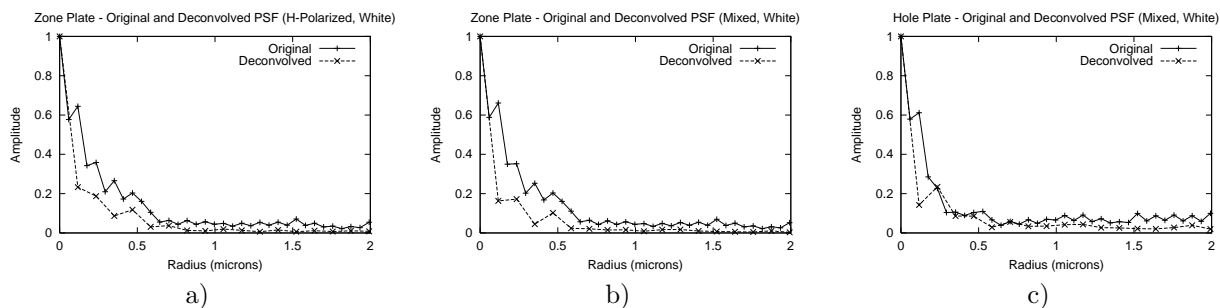


Figure 16. Original and deconvolved modulation transfer functions for a) a zone plate with polarized white light, b) a zone plate with mixed white light, and c) a hole plate with mixed white light.

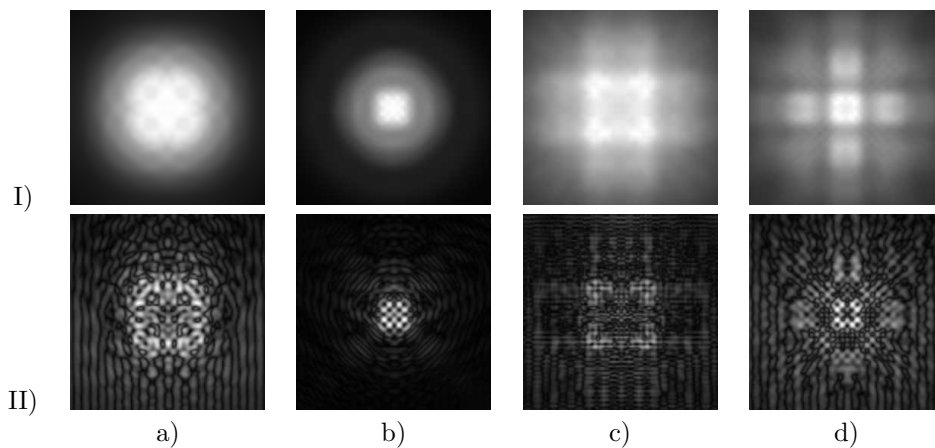


Figure 17. I) Raw and II) processed sensor images. Images a) and b) are formed by a zone plate, and images c) and d) are formed by a hole plate, with mixed-polarization white light. Images a) and c) depict a large checkered test pattern, and images b) and d) depict a small checkered test pattern.

about 0.1 rad, while resolution perpendicular to this axis is about 0.16 rad. This complicates deconvolution, as the polarization of incident light is variable, which means the point spread function isn't precisely known.

A new optical element is proposed, consisting of a plate with small holes arranged in a zone plate pattern. This hole plate is demonstrated to have a point spread function that is insensitive to incident light polarization. Uncorrected image resolution with this hole plate sensor is about 0.16 rad, with some spurious images formed due to secondary peaks in the point spread function. As the point spread function is known, it can be deconvolved more readily than that of the Fresnel zone plate. This improvement comes at the cost of reduced photosensitivity, due to less light passing through the optical element.

Wiener deconvolution can be applied to flatten the modulation transfer function of both zone plates and hole plates. This results in an angular resolution of approximately 0.1 rad, though noise is a concern in images with large angular extent. Artifacts in the hole plate's point spread function are removed sufficiently that it can be used to form legible images, confirming the hole plate's usefulness as an optical element that is insensitive to polarization effects.

REFERENCES

1. S.-G. Wu, D.-N. Yaung, C.-H. Tseng, H.-C. Chien, C. S. Wang, Y.-K. Hsiao, C.-K. Chang, and B. J. Chang, "High performance 0.25- μm cmos color imager technology with non-silicide source/drain pixel," in *IEEE Electron Devices Meeting Technical Digest, International*, pp. 705–708, December 2000.
2. M. Furumiya, K. Hatano, I. Murakami, T. Kawasaki, C. Ogawa, and Y. Nakashiba, "A 1/3-in 1.3 m-pixel single-layer electrode ccd with a high-frame-rate skip mode," in *IEEE Transactions on Electron Devices*, **48**, pp. 1915–1921, September 2001.
3. H. Sagberg, M. Lacolle, I.-R. Johansen, O. Løvhaugen, R. Belikov, O. Solgaard, and A. S. Sudbø, "Micromechanical gratings for visible and near-infrared spectroscopy," in *IEEE Journal of Selected Topics in Quantum Electronics*, **10**, pp. 604–613, May-June 2004.
4. T. Nirmaier, C. A. Diez, and J. F. Billie, "High-speed cmos wavefront sensor with resistive-ring networks of winner-take-all circuits," in *IEEE Journal of Solid-State Circuits*, **40**, pp. 2315–2322, November 2005.
5. J. Tanida and K. Yamada, "Tombo: Thin observation module by bound optics," in *IEEE Lasers and Electro-Optics Society*, pp. 233–234, November 2002.
6. C. Thomas and R. Hornsey, "An image sensor with on-die diffractive optics in 0.18 micron bulk cmos," in *IS&T/SPIE 18th Annual Symposium on Electronic Imaging Science and Technology*, January 2006. Paper no. 6068-06.
7. C. Thomas and R. Hornsey, "A diffractive multispectral image sensor with on- and off-die signal processing and on-die optics in 0.18 micron cmos," in *IS&T/SPIE 19th Annual Symposium on Electronic Imaging Science and Technology*, January 2007. Paper no. 6501-27.
8. M. Born and E. Wolf, *Principles of Optics*, Pergamon Press, 3rd ed., 1965.
9. R. Gonzalez and R. Woods, *Digital Image Processing*, 2nd ed.